International Journal of Heat and Mass Transfer 122 (2018) 1255–1263

Contents lists available at ScienceDirect

International Journal of Heat and Mass Transfer

journal homepage: www.elsevier.com/locate/ijhmt

Thermal and velocity slip effects on Casson nanofluid flow over an inclined permeable stretching cylinder via collocation method

M. Usman [a], Feroz Ahmed Soomro [b], Rizwan Ul Haq [c,d,*], W. Wang [a], Ozlem Defterli [e]

[a] School of Mathematical Sciences, Peking University, Beijing 100871, China
[b] Department of Mathematics, Nanjing University, Nanjing 210093, China
[c] Department of Electrical Engineering, Bahria University, Islamabad, Pakistan
[d] Department of Mechanical and Material Engineering, UWO, London, Canada
[e] Department of Mathematics, Faculty of Art and Sciences, Cankaya University, Main Campus, 06790 Etimesgut-Ankara, Turkey

ARTICLE INFO

Article history:
Received 27 December 2017
Received in revised form 10 February 2018
Accepted 12 February 2018

Keywords:
Inclined stretching cylinder
Slip flow
Nanofluid
Numerical solution
Collocation method

ABSTRACT

The main emphasis of present work is to investigate the velocity and thermal slip effects on Casson nanofluid with heat and mass transfer phenomena over an inclined permeable stretching cylinder. The cylinder is subject to transverse magnetic field. Buongiorno's model is adapted to study the Brownian motion and thermphoresis effects which play a dominant role in nanofluid. Governing set of equations are derived in terms of partial differential equations for Casson nanofluid model, consisting continuity, momentum, energy and concentration equation which are transformed into set of coupled nonlinear ordinary differential equations using similarity transformation. The numerical solution is obtained using collocation method. The literature survey shows that the present problem has not been studied before. Physical quantities of interest are nanofluid velocity, temperature, concentration, skin friction coefficient, Nusselt number and Sherwood number which are analyzed through graphs against the emerging physical parameters. It is found that *Nb* and *Nt* play a dominant role within the thermal and concentration boundary layer regions. In the same manner, suction parameter and both velocity and thermal slip parameters depicts the dynamic effects in the entire domain of stretching surface of the cylinder.

1. Introduction

Nanofluid is the composite of nano-sized particles, like, copper, silver, gold, carbon nanotubes, etc. into the base fluids, like, water, engine oil, glycerin, etc. Literature depicts that Choi and Eastman [1] were firstly gave the idea of utilizing fluid consists of base fluid and nano-sized particles and name it as nanofluid. Previously, it is reported both numerically as well as experimentally that the thermal conductivity of nanofluids is significantly higher than that of conventional base fluids [2]. As a result, the nanofluid got great importance in range of applications. For example, among numerous applications, heat transfer mechanisms, drug delivery, geothermal processes miniature technology are few of them. One can find the further applications related to nanofluids in [3]. We will restrict our attention to the application of flow, heat and mass transfer of nanofluids over stretching surface. Recently, Soomro et al. [4] reported the numerical study of water based carbon nanotubes nanofluid over inclined stretching surface. Passive control of nanoparticles using the non-Newtonian nanofluids flow over linear stretching sheet was studied numerically by Soomro et al. [5]. The flow along converging/diverging channel using nanofluids was studied by Usman et al. [6]. Two different types of nanofluids, *Cu*-water and *Ag*-water, were studied.

The fluids are mainly classified into two categories: Newtonian and Non-Newtonian. Water, engine oil, etc. are the examples of Newtonian fluid which possess linear stress-strain relationship whereas honey, paste, paint, etc. are the examples of non-Newtonian fluids which possess nonlinear stress-strain relationship. Such kinds of fluids are encountered by us in our daily life. So, the study of such fluids is very crucial. In the present research work we will focus on the study of non-Newtonian fluid. Various mathematical models have been proposed for the flow, heat and mass transfer of non-Newtonian fluid. For example: Prandtl fluid model [5,7]; Casson fluid model [8]; Carreau fluid model [9]; Maxwell fluid [10].

Flow due to many kinds of stretching surfaces has been reported in the literature. Khan et al. [11] studied the heat transfer

* Corresponding author at: Department of Electrical Engineering, Bahria University, Islamabad, Pakistan.
E-mail addresses: rizwanulhaq.buic@bahria.edu.pk, ideal_riz@hotmail.com (R. Ul Haq).

https://doi.org/10.1016/j.ijheatmasstransfer.2018.02.045
0017-9310/

characteristics of fluid flow over linearly stretching sheet. Three-dimensional stagnation-point flow over exponential stretching sheet was studied by Rehman et al. [12]. MHD non-Newtonian fluid flow over nonlinear radially stretching surface was taken into consideration by Besthapu et al. [13]. Flow along the vertical stretching sheet stretched exponentially was studied by Besthapu et al. [14]. Malik et al. [15] studied the non-Newtonian fluid flow over exponentially stretching vertical cylinder. Mixed convection flow over stretching cylinder stretched linearly was reported by Imtiaz et al. [16].

Various velocity-slip flow models have been devised during past decades; however, few widely used ones are Maxwell's first-order velocity-slip flow model [17], second-order velocity-slip flow model [18], and Fukui-Kaneko velocity-slip flow model [19], 1.5-order velocity-slip flow model [20]. They all have origin from kinetic theory of gases. Among them, the Fukui-Kaneko model is sufficiently accurate but since it depends highly on geometry and parameters of the flow it is not used in common practice. The first-order, second-order and fractional (1/2) order velocity slip models works very well in the situations when Kundsen number is less than one. That is why these models are widely used in engineering applications. Recently Lin Wu [21] introduced improved second-order slip model which is much reliable and accurate than FK model. It is better in a sense that it can be used for whole range of Kundsen number. To better understand the characteristics of flow, many researchers has studied Wu's model under different physical parameters. Literature shows that Much less attention has been paid to the thermal slip effects on the flow and heat transfer over stretching surface. Ibrahim and Shankar [22] studied the three types of slips: velocity, thermal and Solutal, due to the flow of MHD nanofluid past a stretching surface. First order velocity and thermal slip were analyzed by Hayat et al. [22] while considering the unsteady fluid flow over stretching surface.

The detailed survey of literature shows that the velocity and thermal slip flow of Casson nanofluid over permeable inclined stretching cylinder has not been investigated so far. So, the purpose of present research work is to study non-Newtonian Casson nanofluid flow over permeable inclined stretching cylinder with velocity and thermal slip. Buongiorno's model has been used to study the nanofluid characteristics. The mathematical model is proposed in the form of partial differential equations. Similarity transformation is applied to convert them into similarity equations. Numerical solution is sought using Collocation method. The efficiency of method is presented using error analysis. Physical quantities are analyzed against the varying pertinent parameters using graphs.

2. Problem formulation

Consider the two-dimensional Casson nanofluid flow over a permeable stretching cylinder that makes an angle of α with horizontal axis. The cylinder is stretched at the velocity of $u_w(x) = ax/L$ and the surface temperature is set as $T_w(x) = T_\infty + bx/L$, where a and b is the arbitrary constant, L is the characteristic length and T_∞ denotes the free stream temperature. The graphical representation of the considered physical model is given in Fig. 1. Under the considered assumptions and applying Boussinesq approximations, the governing equations may be written as:

$$\frac{\partial(ru)}{\partial x} + \frac{\partial(rv)}{\partial r} = 0, \tag{1}$$

$$u\frac{\partial u}{\partial x} + v\frac{\partial u}{\partial r} = \vartheta_f\left(1+\frac{1}{\beta}\right)\left(\frac{\partial^2 u}{\partial r^2} + \frac{1}{r}\frac{\partial u}{\partial r}\right) + g(\beta_T(T-T_\infty) + \beta_C(C-C_\infty))\cos\alpha - \frac{\sigma B_0^2}{\rho}u, \tag{2}$$

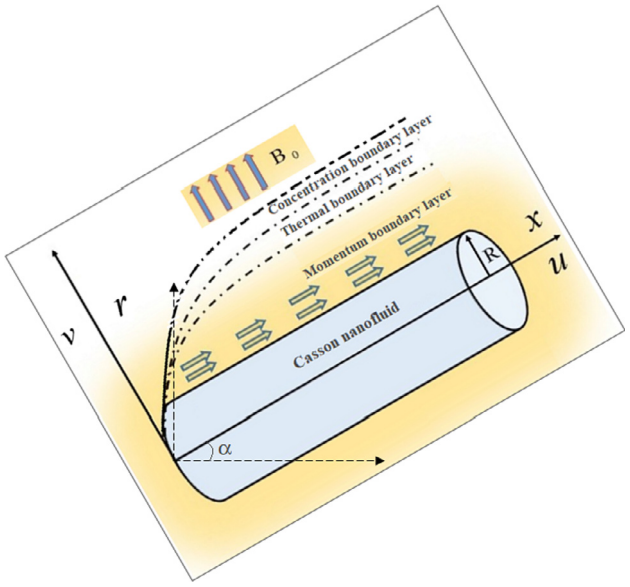

Fig. 1. Geometry of the model.

$$u\frac{\partial T}{\partial x} + v\frac{\partial T}{\partial r} = \alpha^*\left(\frac{\partial^2 T}{\partial r^2} + \frac{1}{r}\frac{\partial T}{\partial r}\right) + \tau\left(D_B\frac{\partial T}{\partial r}\frac{\partial C}{\partial r} + \frac{D_T}{T_\infty}\left(\frac{\partial T}{\partial r}\right)^2\right), \tag{3}$$

$$u\frac{\partial C}{\partial x} + v\frac{\partial C}{\partial r} = D_B\left(\frac{\partial^2 C}{\partial r^2} + \frac{1}{r}\frac{\partial C}{\partial r}\right) + \frac{D_T}{T_\infty}\left(\frac{\partial^2 T}{\partial r^2} + \frac{1}{r}\frac{\partial T}{\partial r}\right). \tag{4}$$

subject to the boundary conditions:

$$\left.\begin{aligned} &u = u_w + U_{slip},\quad v = V_w,\quad T = T_w + T_{slip},\quad C = C_w(x) \text{ at } r = R,\\ &u \to 0,\ T \to T_\infty,\ C \to C_\infty \text{ as } r \to \infty. \end{aligned}\right\} \tag{5}$$

where r is the radial coordinate, u and v are the velocity components in respective x and r direction, T is the temperature of the fluid in the boundary layer, T_∞ is the temperature of the ambient fluid, g is the acceleration due to gravity, U_{slip} and T_{slip} are the velocity and thermal slip, respectively, given by Rizwan et al. [23]. To nondimensionalize the governing Eqs. (1)–(4), we introduce the following similarity transformation:

$$f(\eta) = \frac{\psi}{xR}\sqrt{\frac{L}{a\vartheta}},\ \theta(\eta) = \frac{T-T_\infty}{T_w-T_\infty},\ \phi(\eta) = \frac{C-C_\infty}{C_w-C_\infty},\ \eta = \frac{r^2-R^2}{2R}\sqrt{\frac{a}{L\vartheta}}. \tag{6}$$

where η is the similarity variable, ϑ is the kinematic viscosity and ψ is the stream function which is defined as:

$$u = \frac{1}{r}\frac{\partial\psi}{\partial r},\ v = -\frac{1}{r}\frac{\partial\psi}{\partial x}. \tag{7}$$

Utilizing definition of stream function (7) and similarity variables (6) the governing Eqs. (1)–(4) along with boundary conditions (5) now may be written in nondimensional form as:

$$\left(1+\frac{1}{\beta}\right)((1+2c\eta)f''' + 2cf'') + ff'' - f'^2 + \varepsilon(\theta + R\phi)\cos\alpha - Mf' = 0, \tag{8}$$

$$\frac{1}{Pr}((1+2c\eta)\theta'' + 2c\theta') + f\theta'' + (1+2c\eta)(Nb\theta'\phi' + Nt\theta'^2) = 0, \tag{9}$$

$$(1+2c\eta)\phi'' + 2c\phi' + Le\,Prf\phi' + \frac{Nt}{Nb}((1+2c\eta)\theta'' + 2c\theta') = 0. \tag{10}$$

subject to the boundary conditions:

$$\left.\begin{array}{l} f(\eta=0)=S,\ f'(\eta=0)=1+\lambda f''(\eta=0),\\ \theta(\eta=0)=1+\delta\theta'(\eta=0),\ \varphi(\eta=0)=1,\\ f'(\eta\to\infty)=0,\ \theta(\eta\to\infty)=0,\quad \phi(\eta\to\infty)=0. \end{array}\right\} \tag{11}$$

where prime denotes differentiation with respect to η and the emerging physical parameters are defined as: c is the curvature parameter, ε is the buoyancy force due to temperature difference, ε^* is the buoyancy force due to concentration difference, R is the ratio between ε^* and ε, $(Gr)_c$ is the Solutal Grashof number, $(Gr)_t$ is the thermal Grashof number, Re_x is the Reynolds number, α is the angle of inclination, M is the Hartmann number, Pr is the Prandtl number, Nb is the Brownian motion parameter, Nt is the thermophoresis parameter, Le is the Lewis number, S is the suction ($S>0$) or injection ($S<0$) parameter, λ is the velocity slip parameter and δ is the thermal slip parameter. Above mentioned parameters are defined as:

$$c=\sqrt{\frac{L\nu_f}{aR^2}},\quad \varepsilon=\frac{(Gr)_t}{(Re_x)^2},\quad \varepsilon^*=\frac{(Gr)_c}{(Re_x)^2},\quad (Gr)_c=\frac{g(\beta_c(C-C_\infty)x^3)}{\vartheta^2},$$

$$(Gr)_t=\frac{g(\beta_t(T-T_\infty)x^3)}{\vartheta^2},\quad Re_x=\frac{u_w(x)x}{\vartheta},\quad M=\frac{\sigma B_0^2L}{\rho a},\quad Pr=\frac{\vartheta}{\alpha},$$

$$Nb=\frac{(\rho c)_pD_B(C_w-C_\infty)}{\vartheta(\rho c)_f},$$

$$Nt=\frac{(\rho c)_pD_T(T_w-T_\infty)}{\vartheta T_\infty(\rho c)_f},\quad Le=\frac{a}{D_B},\quad S=-v_w\sqrt{\frac{L}{a\vartheta}},\quad \lambda=a_1\sqrt{\frac{a}{L\vartheta}},$$

$$\delta=c_1\sqrt{\frac{a}{L\vartheta}}.$$

Apart from nanofluid velocity, temperature and nanoparticle concentration other quantities of interest are drag along the cylinder surface, heat transfer rate and mass transfer rate which are given by coefficient of skin friction, Nusselt number and Sherwood number, respectively. The mathematical form of such quantities is given by:

$$c_f=\frac{\tau_w}{\rho u_w^2},\quad Nu=\frac{xq_w}{k(T_w-T_\infty)},\quad Sh=\frac{xq_m}{D_B(C_w-C_\infty)}. \tag{12}$$

where, τ_w, q_w and q_m are the stress tensors, heat flux and mass flux, respectively, and are defined as:

$$\tau_w=\mu\left(1+\frac{1}{\beta}\right)\left(\frac{\partial u}{\partial y}\right)_{y=0},\quad q_w=-k\left(\frac{\partial T}{\partial y}\right)_{y=0},\quad q_m=-D_B\left(\frac{\partial C}{\partial y}\right)_{y=0}. \tag{13}$$

Using (13), dimensionless form of Eq. (12) reduced skin friction coefficient, Nusselt number and Sherwood numbers and are defined as:

$$Re_x^{1/2}c_f=\left(1+\frac{1}{\beta}\right)f''(0),\quad Re_x^{-1/2}Nu=-\theta'(0),\quad Sh\,Re_x^{-1/2}=-\phi'(0). \tag{14}$$

3. Numerical procedure: collocation method

This section presents the analysis of the collocation method [24–26] to investigate the solutions of the problem (8)–(11). This method consists of the following steps:

Step 1. Consider the equations (8)–(10) as:

$$\left(1+\frac{1}{\beta}\right)((1+2c\eta)f'''+2cf'')+ff''-f'^2+\varepsilon(\theta+R\phi)\cos\alpha-Mf'=0, \tag{15}$$

$$\frac{1}{Pr}((1+2c\eta)\theta''+2c\theta')+f\theta'+(1+2c\eta)(Nb\theta'\phi'+Nt\theta'^2)=0, \tag{16}$$

$$(1+2c\eta)\phi''+2c\phi'+Le\,Prf\phi'+\frac{Nt}{Nb}((1+2c\eta)\theta''+2c\theta')=0. \tag{17}$$

Step 2. The next step in this method to choose the trial solution for solving the above system. Let us assume the following trial solutions:

$$\tilde{f}(\eta)=p_1+p_2\eta+p_3\eta^2+\ldots+p_M\eta^M=\sum_{k=1}^{M}p_k\eta^k, \tag{18}$$

$$\tilde{\theta}(\eta)=p_{M+1}+p_{M+2}\eta+p_{M+3}\eta^2+\ldots+p_{2M}\eta^M=\sum_{k=1}^{M}p_{k+M}\eta^k, \tag{19}$$

$$\tilde{\varphi}(\eta)=p_{2M+1}+p_{2M+2}\eta+p_{2M+3}\eta^2+\ldots+p_{3M}\eta^M=\sum_{k=1}^{M}p_{k+2M}\eta^k, \tag{20}$$

In above M is denote the convergence control parameter, as M increases solutions get faster convergent. Imposing the boundary conditions (11) into trial solutions (18)–(20), the reduced trial solutions achieved as:

$$\tilde{f}(\eta)=S+\left(1-\frac{\lambda}{\lambda+\eta_\infty}\right)\eta-\frac{1}{2}\frac{1}{\lambda+\eta_\infty}\eta^2+\sum_{k=1}^{M}p_k\left(\eta^{k+2}-\frac{(k+2)}{2}\frac{\eta_\infty^{k+1}}{\lambda+\eta_\infty}\eta^2-\frac{(k+2)\lambda\eta_\infty^{k+1}}{\lambda+\eta_\infty}\eta\right), \tag{21}$$

$$\tilde{\theta}(\eta)=1-\frac{\delta}{\delta+\eta_\infty}-\frac{1}{\delta+\eta_\infty}\eta+\sum_{k=1}^{M}p_{k+M}\left(\eta^{k+1}-\frac{\delta\eta_\infty^{k+1}}{\delta+\eta_\infty}\eta^2-\frac{\delta\eta_\infty^{k+1}}{\delta+\eta_\infty}\eta\right), \tag{22}$$

$$\tilde{\phi}(\eta)=1-\frac{1}{\eta_\infty}\eta+\sum_{k=1}^{M}p_{k+2M}(\eta^k-\eta_\infty^k)\eta. \tag{23}$$

Step 3. Residual of velocity, temperature and concentration attained as follow by substituting the trial solutions (21)–(23) into to Eqs. (15)–(17):

$$R_f=\left(1+\frac{1}{\beta}\right)\left((1+2c\eta)\tilde{f}'''+2c\tilde{f}''\right)+\tilde{f}\tilde{f}''-\tilde{f}'^2+\varepsilon\left(\tilde{\theta}+R\tilde{\phi}\right)\cos\alpha-M\tilde{f}'\neq 0,$$

$$R_\theta=\frac{1}{Pr}\left((1+2c\eta)\tilde{\theta}''+2c\tilde{\theta}'\right)+\tilde{f}\tilde{\theta}'+(1+2c\eta)\left(Nb\tilde{\theta}'\tilde{\phi}'+Nt\tilde{\theta}'^2\right)\neq 0,$$

$$R_\phi=(1+2c\eta)\tilde{\phi}''+2c\tilde{\phi}'+Le\,Pr\tilde{f}\tilde{\phi}'+\frac{Nt}{Nb}\left((1+2c\eta)\tilde{\theta}''+2c\tilde{\theta}'\right)\neq 0.$$

Step 4. Discretize the above residuals at $\eta_i=\frac{i}{M}$, where $i=0,1,2,\ldots,M-1$, we achieved the system of algebraic equations.

Step 5. After solving the system of algebraic equations obtained in last step we get the values of p_i 's. Setting these constants into the reduced trial solutions we get the approximate solutions of the problem (8)–(11).

4. Results and discussion

Effect of emerging parameters i.e., magnetic parameter M, Casson fluid parameter β, curvature parameter c, buoyancy force parameter ε, inclination parameter α, ratio parameter R, suction/

injection parameter S, velocity slip parameter λ, Prandtl number Pr, Brownian motion parameter Nb, thermophoresis parameter Nt, thermal slip parameter δ and Lewis number Le on non-dimensional velocity $f'(\eta)$, temperature $\theta(\eta)$ and concentration $\phi(\eta)$ profiles are discussed in this section. Influence of these parameters portrayed in Figs. 2–11 along with detailed discussion. Behavior of skin friction coefficient, Nusselt number and Sherwood number due to the variation in various parameters is also deliberated in Figs. 12–14. Table 1 construct to study the square residual error. For convenience we divide this section into subsections as: first subsection is about the impact of various parameters on the velocity field. Effect of curvature parameter, Prandtl number, inclination parameter, thermophoresis parameter, Brownian motion parameter and thermal slip parameter on the temperature profile is deliberated in second subsection. Behavior of concentration profiles under the influence of numerous parameters shown in third subsection and last subsection devoted to the study of physical quantities and analysis of square residual error.

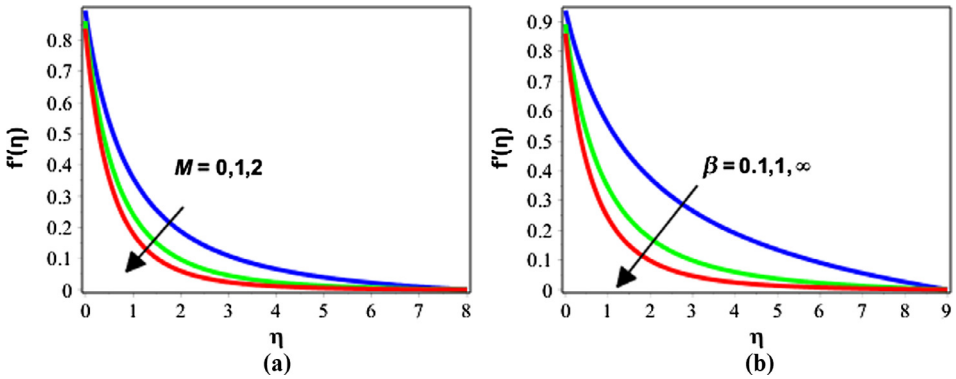

Fig. 2. Variation in $f'(\eta)$ due to (a) M when $\beta = \infty$ and (b) β when $M = 1$ while rest parameters are $S = 0.2, Pr = 6.0, Nb = R = \delta = c = 0.5, Nt = 0.3, \lambda = \varepsilon = 0.1$, $Le = 1.0, \alpha = 3^o$.

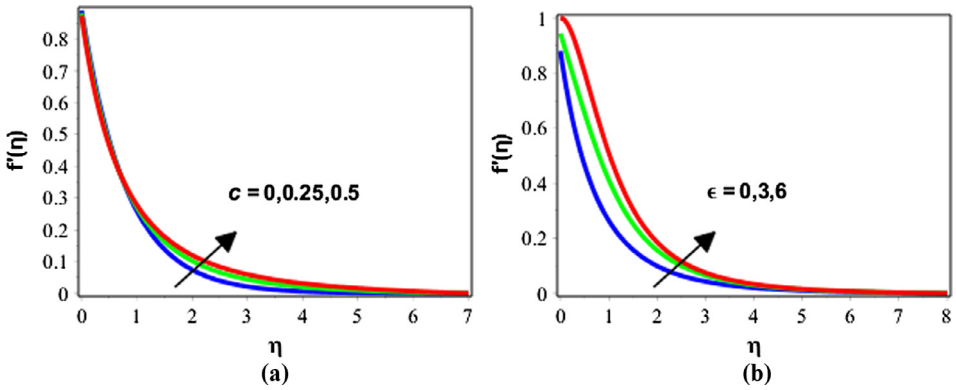

Fig. 3. Variation in $f'(\eta)$ due to (a) c when $\varepsilon = 0.1$ and (b) ε when $c = 0.5$ while rest parameters are $S = 0.2, Pr = 6.0, Nb = R = \delta = 0.5, Nt = 0.3, \lambda = 0.1$, $Le = \beta = 1.0, \alpha = 3^o, M = 2.0$.

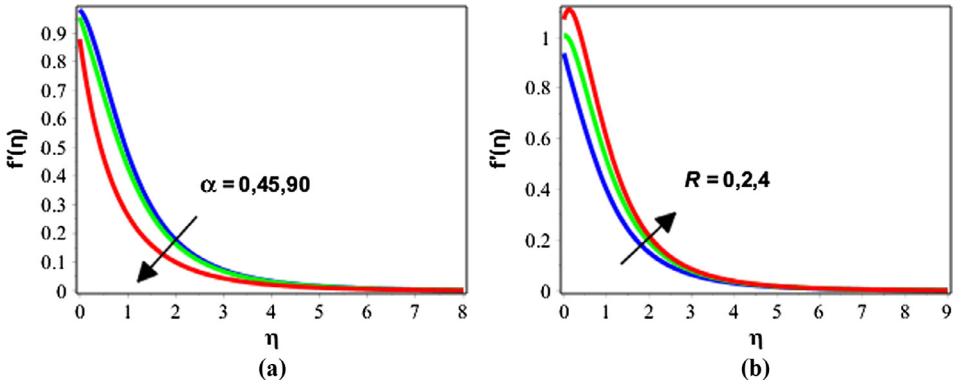

Fig. 4. Variation in $f'(\eta)$ due to (a) α when $R = 0.5$ and (b) R when $\alpha = 45^o$ while rest parameters are $S = 0.2, Pr = 6.0, Nb = \delta = 0.5, Nt = 0.3, \lambda = 0.1$, $Le = \beta = 1.0, \varepsilon = 5.0, M = 2.0, c = 0.25$.

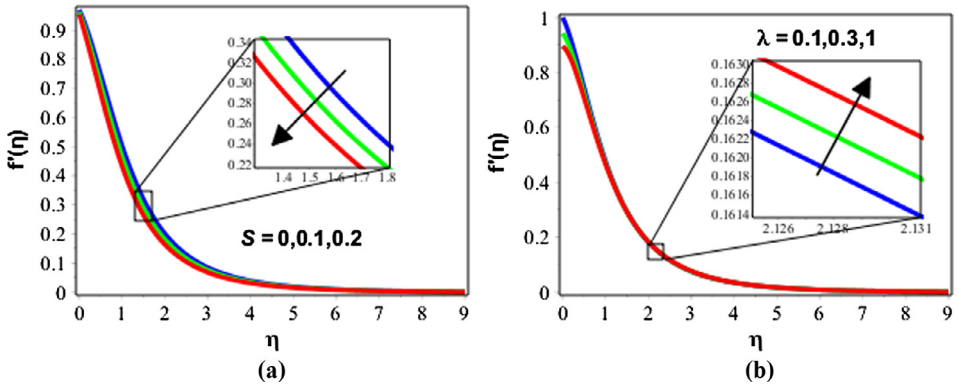

Fig. 5. Variation in $f'(\eta)$ due to (a) S when $\lambda = 0.1$ and (b) λ when $S = 0.2$ while rest parameters are $Pr = 3.97, Nb = \delta = R = 0.5, Nt = 0.3, Le = \beta = 1.0, \varepsilon = 5.0$, $\alpha = 5^o, M = 2.0, c = 0.25$.

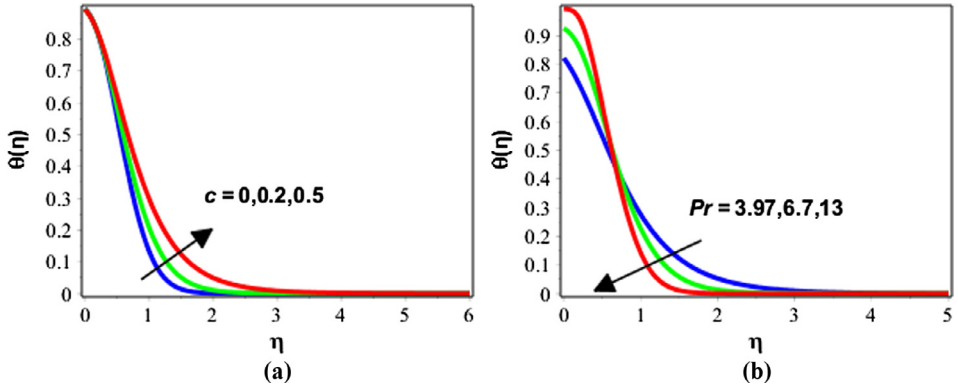

Fig. 6. Variation in $\theta(\eta)$ due to (a) c when $Pr = 3.97$ and (b) Pr when $c = 0.3$ while rest parameters are $\alpha = 45^o, Nb = \delta = R = 0.5, Nt = 0.3, Le = \beta = 1.0, M = 2.0$, $\lambda = 0.1, \varepsilon = 1.0, S = 0.2$.

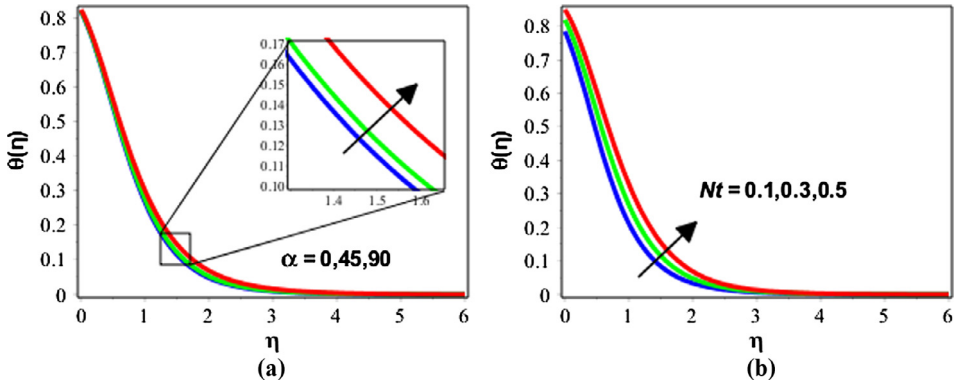

Fig. 7. Variation in $\theta(\eta)$ due to (a) α when $Nt = 0.3$ and (b) Nt when $\alpha = 5^o$ while rest parameters are $Pr = 3.97, Nb = \delta = R = 0.5, Le = \beta = 1.0, M = 2.0, \lambda = 0.1$, $\varepsilon = 1.0, S = 0.2, c = 0.3$.

4.1. Behavior of velocity profiles

Figs. 2–5 are portrayed to execute the behavior of velocity profile for different values of emerging parameters. Fig. 2 illustrates the variation in $f'(\eta)$ due to the variation in Hartmann number and Casson parameter. Velocity field demonstrate the decreasing behavior as up surging Hartmann number and Casson parameter. Hartman number represents the ratio of electromagnetic force to the viscous force and magnetic field is applied in the opposite direction of the fluid, therefore as enhancing Hartmann number reasons decreasing the velocity field. Effect of curvature and buoyancy force parameters on dimensionless velocity profile is established in Fig. 3. As increasing curvature and buoyancy force parameters, velocity profile increases gradually. Effect of buoyancy parameter is more dominant than the curvature parameter. Fig. 4 plotted to depict the variation in velocity profile against the variation in inclination and ratio parameters. Velocity profile decreases as angle of inclination increases. For small value of inclination parameter behavior of velocity profile is insignificant. On the other hand, as increasing the ratio parameter velocity profile increases gradually. Variation in velocity field for different values of injection and velocity slip parameters explained in Fig. 5. Behavior of veloc-

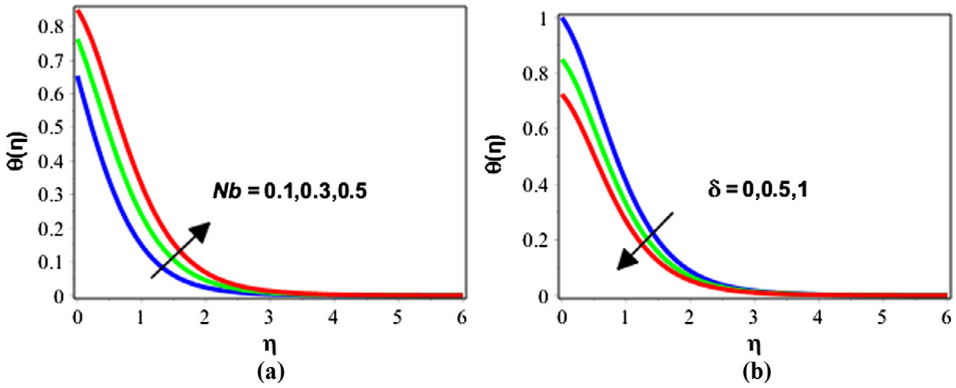

Fig. 8. Variation in $\theta(\eta)$ due to (a) Nb when $\delta = 0.5$ and (b) δ when $Nb = 0.5$ while rest parameters are $Pr = 3.97, \delta = R = 0.5, Nt = 0.5, Le = \beta = 1.0, M = 2.0, \lambda = 0.1, \varepsilon = 1.0, S = 0.2, c = 0.3$.

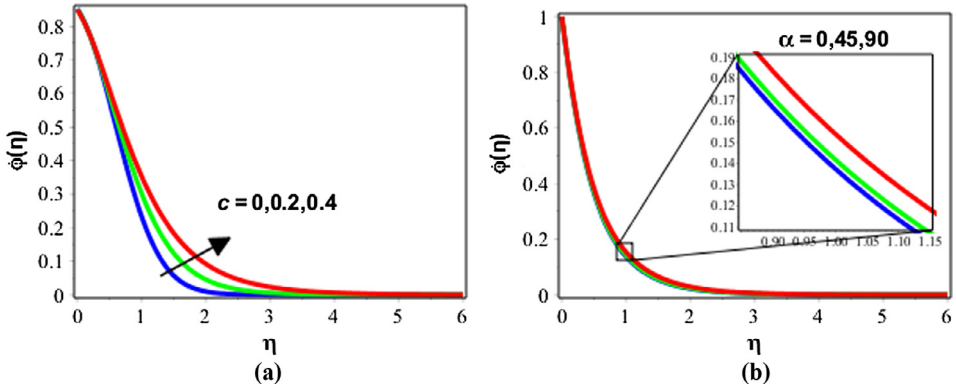

Fig. 9. Variation in $\phi(\eta)$ due to (a) c when $\alpha = 5^o$ and (b) α when $c = 0.2$ while rest parameters are $Pr = 3.97, Nt = Nb = \delta = R = 0.5, Le = \beta = 1.0, M = 2.0, \lambda = 0.1, \varepsilon = 1.0, S = 0.2$.

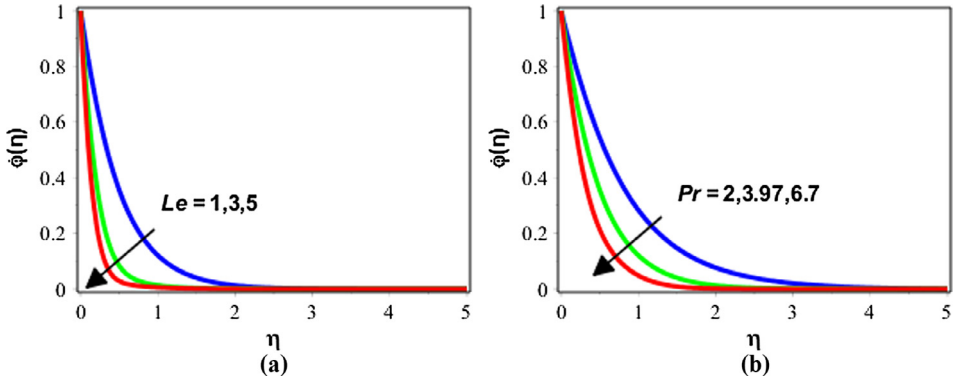

Fig. 10. Variation in $\phi(\eta)$ due to (a) Le when $Pr = 3.97$ and (b) Pr when $Le = 1.0$ while rest parameters are $\alpha = 5^o, Nb = \delta = R = 0.5, \beta = 1.0, M = 2.0, \lambda = Nt = 0.1, c = 0.25, \varepsilon = 1.0, S = 0.2$.

ity profile is inversely proportional to the injection parameter. Contrary behavior is achieved for suction parameter. Insignificant increment has been observed against increasing the velocity slip parameter.

4.2. Behavior of temperature profiles

Variation in temperature distribution due to the variation in curvature parameter, Prandtl number, inclination parameter, thermophoresis parameter, Brownian motion parameter and thermal slip parameter is represented in Figs. 6–8. Fig. 6 pondered the influence of curvature parameter and Prandtl number on temperature distribution. Temperature of the fluid increases as increases the curvature parameter. On the other side, behavior of the temperature distribution is obtained under the impact of Prandtl number. Temperature profile increases as increases the Prandtl number when $\eta \in [0, 0.7]$ and decreases when $[0.7, 5]$. Impact of inclination parameter and the thermophoresis parameter on the fluid temperature deliberated in Fig. 7. It is observed that temperature of the fluid increases under the influence of both inclination and the thermophoresis parameters. Effect of thermophoresis parameter is clearer. Variation in temperature distribution for different values

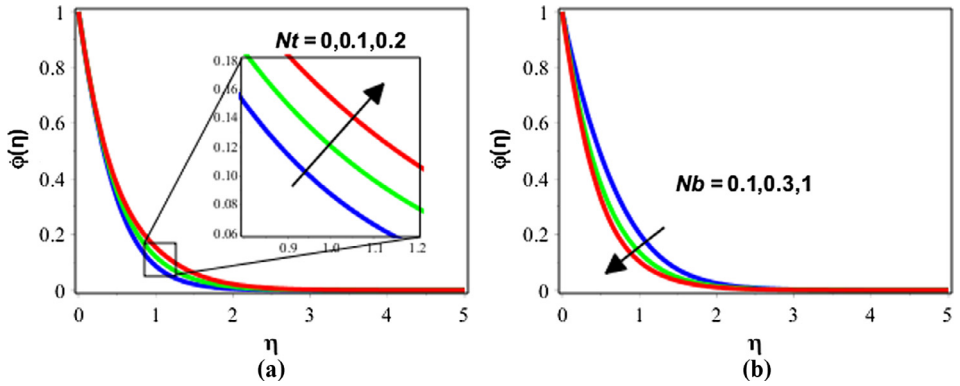

Fig. 11. Variation in $\phi(\eta)$ due to (a) Nt when $Nb = 0.5$ and (b) Nb when $Nt = 0.1$ while rest parameters are $\alpha = 5^o, Pr = 3.97, \delta = R = 0.5, \beta = 1.0, M = 2.0, \lambda = 0.1, c = 0.25, Le = 1.0, \varepsilon = 1.0, S = 0.2$.

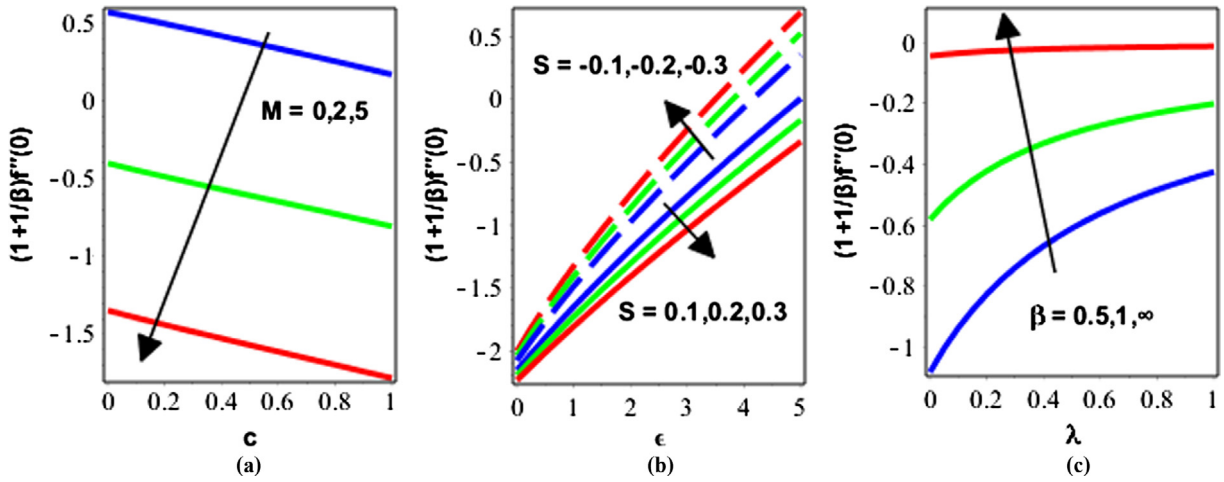

Fig. 12. Behavior of skin friction coefficient due to (a) M and c when $S = 0.2, \varepsilon = 5.0, \beta = 1.0, \lambda = 0.1$ (b) S and ε when $M = 2.0, c = 0.2, \beta = 1.0, \lambda = 0.1$ (c) β and λ when $S = 0.2, \varepsilon = 5.0, M = 2.0, c = 0.1$ while rest parameters are $\alpha = 5^o, Pr = 3.97, R = Nb = \delta = 0.5, Le = 1.0, Nt = 0.1$.

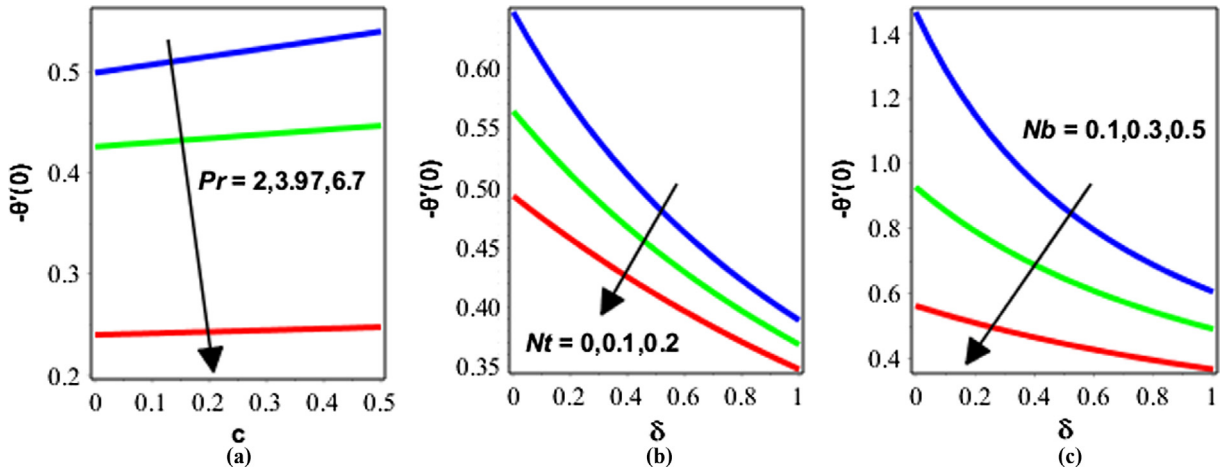

Fig. 13. Behavior of skin friction coefficient due to (a) Pr and c when $Nt = 0.1, \delta = 0.5, Nb = 0.5$ (b) Nt and δ when $Pr = 3.97, c = 0.5, Nb = 0.5$ (c) Nb and δ when $Nt = 0.1, c = 0.5, Pr = 3.97$ while rest parameters are $\alpha = 5^o, M = \varepsilon = 2.0, R = 0.5, Le = \beta = 1.0, \lambda = 0.1, S = 0.2$.

of Brownian motion parameter and thermal slip parameter is shown in Fig. 8. As enhancing the Brownian motion parameter temperature profiles increase gradually. The contrary behavior of temperature distribution is achieved as enhancing the thermal slip parameter i.e., temperature of the fluid decreases as increasing thermal slip parameter.

4.3. Behavior of concentration profiles

Behavior of dimensionless concentration profile under the effects of numerous parameters pondered in Figs. 9–11. Fig. 9 analyze the behavior of curvature and inclination parameters on the dimensionless concentration profile. Concentration profiles are

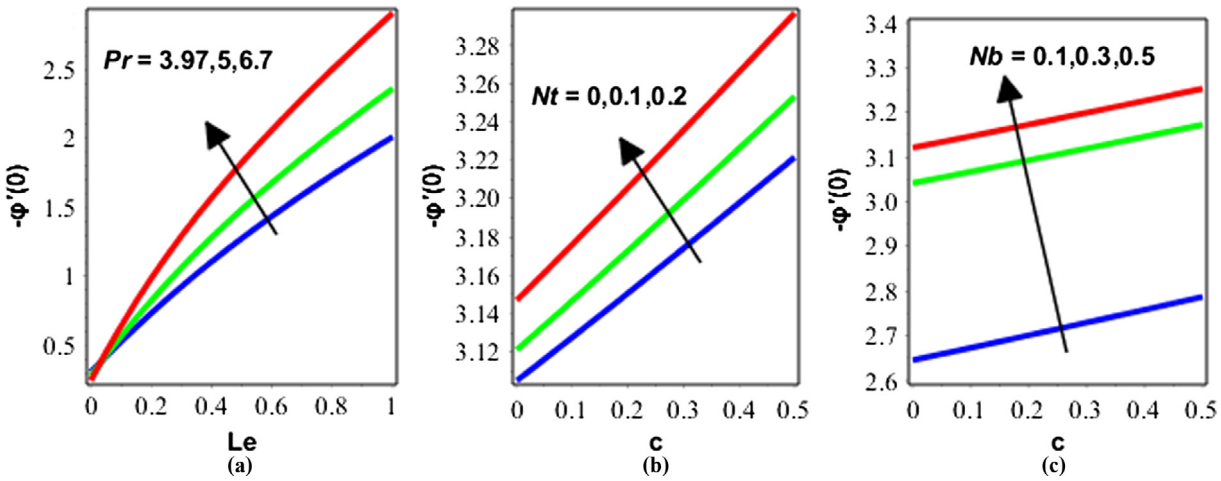

Fig. 14. Behavior of skin friction coefficient due to (a) Pr and Le when $Nt = 0.1, c = 0.5, Nb = 0.5$ (b) Nt and c when $Pr = 3.97, Le = 2.0, Nb = 0.5$ (c) Nb and c when $Nt = 0.1, Le = 2.0, Pr = 3.97$ while rest parameters are $\alpha = 5^o, M = \varepsilon = 2.0, R = 0.5, Le = \beta = 1.0, \lambda = 0.1, S = 0.2$.

Table 1
Square residual error for different order approximations.

M	Δ_f	Δ_θ	Δ_ϕ
5	1.4510E−05	3.2587E−04	1.2471E−05
10	2.6540E−12	1.2547E−12	1.2510E−13
15	7.5482E−21	2.0025E−20	6.2540E−22
20	6.5123E−29	3.2154E−38	9.1587E−30
25	4.1150E−35	6.2358E−35	7.6547E−36

directly proportional to curvature and inclination parameters. Effect of small values of inclination parameter on the concentration profile is insignificant. Effect of Lewis number and Prandtl number on the non-dimensional concentration profile is considered in Fig. 10. Concentration profile decreases as increasing both Lewis number and Prandtl number. Effect of small Lewis number on concentration profile is more prominent. Finally, variation in concentration profile due to the variation in Brownian motion and thermophoresis parameters is portrayed in Fig. 11. It is observed that concentration profiles show the increasing behavior against thermophoresis parameter and decreasing behavior against Brownian motion parameter.

4.4. Behavior of skin friction, Nusselt number, Sherwood number and error analysis

Figs. 12–14 are plotted to investigate the effects of several parameters on the physical quantities. Behavior of skin friction coefficient under the effects of Hartmann number, curvature parameter, suction/injection parameter, buoyancy parameter, Casson parameter and thermal slip parameter is revealed in Fig. 12. Skin friction coefficient increases with the increment of buoyancy, thermal, Casson and suction parameters. As upsurge Hartmann number, curvature parameter and injection parameter the skin friction coefficient shows the decreasing behavior. It is noted that behavior of skin friction coefficient against injection and suction cases are opposite which is expected. Effect of Prandtl number, curvature parameter, thermophoresis parameter, Brownian motion parameter and thermal slip parameter on the local Nusselt number is considered in Fig. 13. Nusselt number shows the increasing behavior as increasing curvature parameter and decreasing behavior as increasing Prandtl number, thermophoresis parameter, Brownian motion parameter and thermal slip parameter. Fig. 14 reveal the effects of Prandtl number, Lewis parameter, thermophoresis parameter, Brownian motion parameter and thermal slip parameter on the local Sherwood number. Sherwood number deliberates the increasing behavior against all the above physical parameters.

5. Conclusion

In this article Casson nanofluid flow, heat and mass transfer over permeable inclined stretching cylinder has been investigated. The cylinder is subject to transverse magnetic field. Buongiorno's model is adapted to study the Brownian motion and thermophoresis effects. Viable transforms are used to obtain the set of simplified ODEs. Collocation method is utilized to explore the solutions of these ODEs. Key findings are enlisted below:

- The curvature parameter enhances the velocity, temperature and concentration profiles.
- Skin friction coefficient increases as buoyancy, thermal, Casson and suction parameters increases and decreases as upsurge Hartmann number, curvature parameter and injection parameter.
- Skin friction coefficient against injection and suction cases is opposite which is expected.
- Nusselt number shows the increasing behavior as increasing curvature parameter and decreasing behavior as increasing Prandtl number, thermophoresis parameter, Brownian motion parameter and thermal slip parameter.
- Sherwood number increases as Prandtl number, Lewis parameter, thermophoresis parameter, Brownian motion parameter and thermal slip parameter increases.
- Obtained results show that collocation method is appropriate, well-matched, efficient, accurate and reliable to examine the solution.

Conflict of interest

There is no actual or potential conflict of interest including any financial, personal or other relationships with other people or organizations.

References

[1] Stephen U.S. Choi, J.A. Eastman, Enhancing thermal conductivity of fluids with nanoparticles, in: presented at ASME International Mechanical Engineering Congress and Exposition, 1995.

[2] P. Keblinski, J.A. Eastamn, D.G. Cahill, Nanofluids for thermal transport, Mater. Today 8 (2005) 36–44.
[3] Kaufui Vincent Wong, Applications of nanofluids: current and future, Adv. Mech. Eng. (2010).
[4] Feroz Ahmed Soomro, Rizwan-ul-Haq, Z.H. Khan, Qiang Zhang, Numerical study of entropy generation in MHD water based carbon nanotubes along an inclined permeable surface, Eur. Phys. J. Plus 132 (412) (2017).
[5] Feroz Ahmed Soomro, Rizwan -ul-Haq, Zafar Hayat Khan, Qiang Zhang, Passive control of nanoparticles due to convective heat transfer of Prandtl fluid model at the stretching surface, Chin. J. Phys. 55 (2017) 1561–1568.
[6] Muhammad Usman, Rizwan -ul-Haq, Muhammad Hamid, Wei Wang, Least square study of heat transfer of water based Cu and Ag nanoparticles along a converging/diverging channel, J. Mol. Liq. (2017), https://doi.org/10.1016/j.molliq.2017.11.047.
[7] K. Ganesh Kumar, N.G. Rudraswamy, B.J. Gireesha, Rizwan -ul-Haq, Effects of mass transfer on MHD three dimensional flow of a Prandtl liquid over a flat plate in the presence of chemical reaction, Results Phys. 7 (2017) 3465–3471.
[8] Prabhakar Besthapu, Rizwan Ul Haq, Shankar Bandari, Qasem M. Al-Mdallal, Thermal radiation and slip effects on MHD stagnation point flow of non-Newtonian nanofluid over a convective stretching surface, Neural Comput. Appl. (2017), https://doi.org/10.1007/s00521-017-2992-x.
[9] Hashim, Masood Khan, Ali Saleh Alshomrani, Riwan Ul Haq, Investigation of dual solutions in flow of a non-Newtonian fluid with homogeneous-heterogeneous reactions: Critical points, Eur. J. Mech./B Fluids 68 (2017) 30–38.
[10] N.A. Halim, Rizwan Ul Haq, N.F.M. Noor, Active and passive controls of nanoparticles in Maxwell stagnation point flow over a slipped stretched surface, Meccanica 52 (2017) 1527–1539.
[11] Z.H. Khan, M. Qasim, Rizwan Ul Haq, Qasem M. Al-Mdallal, Closed form dual nature solutions of fluid flow and heat transfer over stretching/shrinking sheet in a porous medium, Chin. J. Phys. 55 (2017) 1284–1293.
[12] Fiaz Ur Rehman, S. Nadeem, R.U. Haq, Heat transfer analysis for three-dimensional stagnation-point flow over an exponentially stretching surface, Chin. J. Phys. 55 (2017) 1552–1560.
[13] Prabhakar Besthapu, Rizwan Ul Haq, Shankar Bandari, Qasem M. Al-Mdallal, Thermal radiation and slip effects on MHD stagnation-point flow of non-Newtonian nanofluid over a convective stretching surface, Neural Comput. Appl. 0 (2017), https://doi.org/10.1007/s00521-017-2992-x.
[14] Prabhakar Besthapu, Rizwan Ul Haq, Shankar Bandari, Qasem M. Al-Mdallal, Mixed convection flow of thermally stratified MHD nanofluid over an exponentially stretching surface with viscous dissipation effect, J. Taiwan Inst. Chem. Eng. 71 (2017) 307–314.
[15] M.Y. Malik, M. Naseer, S. Nadeem, Abdul Rehman, The boundary layer flow of Casson nanofluid over a vertical exponentially stretching cylinder, Appl. Nanosci. 4 (2014) 869–873.
[16] Maria Imtiaz, Tasawar Hayat, Ahmed Alsaedi, Mixed convection flow of Casson nanofluid over a stretching cylinder with convective boundary conditions, Adv. Power Technol. 27 (2016) 2245–2256.
[17] J.C. Maxwell, On stresses in rarified gases arising from inequalities of temperature, Philos. Trans. R. Soc. 170 (1879) 231–256.
[18] Y.T. Hsia, G.A. Domoto, An experimental investigation of molecular rarefaction effects in gas lubricated bearings at ultra-low clearances, J. Lubr. Technol. 105 (1983) 120–129.
[19] S. Fukui, R. Kaneko, A database for interpolation of poiseuille flow rates for high Knudsen number lubrication problems, J. Tribol. 112 (1990) 78–83.
[20] Y. Mitsuya, Modified Reynolds equation for ultra-thin film gas lubrication using 1.5-order slip-flow model and considering surface accommodation coefficient, J. Tribol. 115 (1993) 289–294.
[21] L. Wu, A slip model for rarefied gas flows at arbitrary Knudsen number, Appl. Phys. Lett. 93 (2008) 253103.
[22] Wubshet Ibrahim, Bandari Shankar, MHD boundary layer flow and heat transfer of a nanofluid past a permeable stretching sheet with velocity, thermal and Solutal slip boundary conditions, Comput. Fluids 75 (2013) 1–10.
[23] Rizwan Ul Haq, Sohail Nadeem, Zafar Hayat Khan, Noreen Sher Akbar, Thermal radiation and slip effects on MHD stagnation point flow of nanofluid over stretching sheet, Phys. E: Low-dimensional Syst. Nanostruct. 65 (2015) 17–23.
[24] T. Zhu, S.N. Atluri, A modified collocation method and a penalty formulation for enforcing the essential boundary conditions in the element free Galerkin method, Comput. Mech. 21 (3) (1998) 211–222.
[25] I. Babuska, F. Nobile, R. Tempone, A stochastic collocation method for elliptic partial differential equations with random input data, SIAM J. Numer. Anal. 45 (3) (2007) 1005–1034.
[26] M. Rahimi-Gorji, O. Pourmehran, M. Gorji-Bandpy, D.D. Ganji, An analytical investigation on unsteady motion of vertically falling spherical particles in non-Newtonian fluid by collocation method, Ain Shams Eng. J. 6 (2) (2015) 531–540.